Master 2 Internship report

Université Paris-Cité

Infrared detection with HgTe colloidal quantum dots

by

Tommaso GEMO

Institut des NanoSciences de Paris

Acknowledgements

First of all, I would like to thank Emmanuel, my internship supervisor, for being a phenomenal teacher who followed me closely during these months in his group, I have learned a lot from him, especially on how to efficiently organize my scientific work, and I still have much more to learn. I am grateful for being able to find a mentor with his knowledge, and who was always there to encourage me to reach my objectives.

I am thankful for the amazing members of the OCN group, starting from Adrien and Mariarosa, who were always cheerful in helping me to gain confidence with all the equipment of the lab, and were never hesitant in guiding me through my project, while also being open for more relaxed personal conversations. I would like to thank Dario, Erwan and Huichen for their contribution to the amazing environment that I found at INSP, where I felt welcomed since the day I arrived. I am grateful for meeting Albin and Andrei, my fellow intern colleagues, with whom I was able to share my experience, as well as many interesting and enriching discussions.

I am thankful for Yoann, our chemist engineer, for providing the high-quality nanocrystals on which all of the devices I fabricated were based. I also thank Erwan, the cleanroom engineer at INSP for keeping the cleanroom operative all through these months.

I would like to thank my girlfriend Sara, the sweetest and most inspiring person I am lucky to spend my time with, whose radiant energy helped me to get through the toughest times during my Parisian experience. I am grateful to have met Marco, my roommate, in this short period of time you turned from a complete stranger to one of my dearest friends, and this experience would not have been the same without you. I am also thankful for Eva and Margherita, my other flat mates, who have always been there for me even during the stressful times when sharing a small apartment like ours posed its difficulties.

I am grateful for my friends in Italy (Leonardo, Francesco, Gilberto, Cristina, Niccolò, Francesca) who despite the distance that separates us, have shown their support all through my period of absence, and were always there to spend time together whenever I returned to my hometown.

I would like to express my sincere appreciation to my family (Silvana, Laura, Massimo, Franco, Sara, Giulia, Riccardo; Giovanni and Roberto) who stayed close to me throughout my studies, giving me the motivation to never give up, and always offering a helping hand when I was in need.

I wish to thank my brother Alessandro, who is enduring an arduous challenge with his head held high, and despite the many difficulties, never missed the chance to show me his love and support. I am proud of you, I miss you, and I can't wait to be reunited once again.

Finally, I would like to express my gratitude towards my parents, my biggest fans, who made me the person I am today and made this wonderful experience come true. Words cannot express how blessed I feel for being your son, and for all the love you showed me since I left for my studies, vi voglio un mondo di bene.

Abstract

This report presents an overview on the field of semiconductor nanocrystals, and on their use as the active media in infrared photodetectors. In present days, due to the high cost and low throughput of the techniques for the production of state-of-the-art detectors based on bulk materials or heterostructures, infrared sensing remains limited to few niche applications like astronomy, defense and research. Lately, a new class of materials, has emerged as a promising candidate to be the new go-to active layer in infrared detectors. Colloidal quantum dots exhibit extraordinary properties, among which the band gap tunability, the solution processability and the silicon compatibility, which have raised the interest of the scientific community on the potential employment of this new technology for the production of low-cost sensors. In this report, I will dig into further detail on the physics behind the working principles of a specific type of semiconductor nanocrystals, which are mercury telluride quantum dots. This material, benefitting from its semimetal nature when in bulk form, is known to be the most spectral tunable available for infrared applications. I will dig onto the techniques that allow for the fabrication of optoelectronic devices, and how these are characterized for an evaluation of their performance.

Keywords: infrared, colloidal quantum dots, optoelectronic devices, mercury telluride.

Contents

1 OCN team at INSP

The Institute of NanoSciences of Paris (INSP) is a joint research unit of CNRS and Sorbonne Université, focused on the observation, understanding and control of the properties that materials acquire when their size is reduced down to the nanometric scale. My work was carried out in the "Physical Chemistry" team, and more particularly in the "Optoelectronics of Confined Nanomaterials" (OCN) group.

The focus of the OCN team are functional materials and their potential applications for electronic and optoelectronics; in particular the group led by dr. Emmanuel Lhuillier is currently involved in the design of IR optoelectronic devices (both detectors and emitters) using narrow band gap nanocrystals as the active medium.

The INSP cleanroom and the two gloveboxes allow the fabrication of devices in a controlled environment starting from various available substrates (Glass, Si, SOI, SiO_2), with advanced techniques like e-beam lithography and evaporators for the deposition of both metals and dielectrics. The synthesis of the HgTe NCs is done inside of INSP by Yoann Prado, the chemist engineer of the team. Full characterization of the devices is also done in house, with two cryostats for measurements at low temperature, two Fourier-Transform Infrared (FTIR) spectrometers for absorption and transmission experiments, and electronic setups for measurements of electronic transport with gate, temperature and time resolved possibilities; photocurrent measurements are also feasible with sources from the UV to the MWIR.

The OCN team is composed of 14 members, with three permanent researchers (Emmanuel Lhuillier, Debora Pierucci and James K. Utterback) with support from two engineers (Yoann Prado and Claire Abadie), two post docs (Adrien Khalili and Dario Mastrippolito), four PhD students (Mariarosa Cavallo, Huichen Zhang, Erwan Bossavit and Lam Nguyen Do) and three interns (Albin Colle, Andrei Shcherbakov and myself).

2 General context: Infrared radiation & Colloidal Quantum Dots

Nanocrystals (NCs) have been at the center of attention in the field of nanotechnologies starting from the early 1980s, when researchers began exploring the effects of quantum confinement to unveil new properties of matter. A major breakthrough occurred in 1993, with the publication of a paper from Murray, Norris and Bawendi, in which they reported the synthesis of monodispersed high-quality cadmium chalcogenide (CdE, E = S, Se, Te) colloidal quantum dots[1]. Over the last 10 years, the commercialization of the first quantum dot displays increased the interest of the public on the subject of nanomaterials. This technology is based on cadmium chalcogenides or the less toxic indium phosphide, whose intermediate bulk bandgap can be engineered to cover the whole visible spectrum. Numerous other applications take advantage of the effects of quantum confinement on the optoelectronic properties of semiconductors, and my internship is focused on exploring one of them, in particular infrared (IR) detection. To be more specific, the focus of my work over the last few months has been the mid-wave infrared, as opposed to the more widely-explored near-infrared and short-wave infrared parts of the spectrum. The high cost of available technologies in this field is the motivation for researches to look for cheaper alternatives, with the aim of opening the market to a different audience, other than military and researchers. Among the many candidate materials for IR sensing, mercury telluride (HgTe), thanks to its semimetal nature when in bulk form, is at the center of attention for applications in the mid-wave and long-wave infrared.

2.1 The infrared

The infrared is the portion of the electromagnetic (EM) spectrum whose photons have a shorter wavelength than visible ones; the infrared spectrum is commonly divided into five subregions:

- **Near-infrared (NIR)** relates to wavelengths ranging from 0.7 to 1.4 μm (890 – 1650 meV)
- **Short-wave infrared (SWIR)** covers the range between 1.4 and 3 μm (410 – 890 meV)
- **Mid-wave infrared (MWIR)** is defined for photons in the range 3 to 5 μm (110 – 410 meV)
- **Long-wave infrared (LWIR)** spans the region from 8 to 15 μm (80 – 110 meV)
- **Far infrared (FIR)** deals with all EM radiation with wavelength above 15 μm (1 – 80 meV)

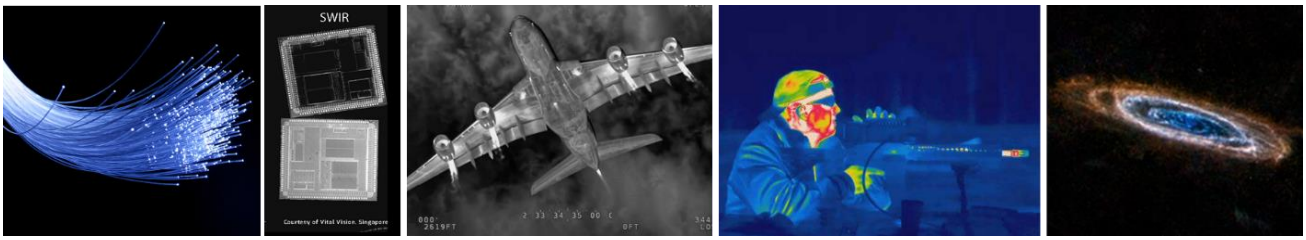

Figure 1: typical applications of the different regions of the infrared spectrum. From left to right: NIR is the typical wavelength for telecommunication, due to the low absorption of optic fibers in this range. SWIR image of a silicon chip, which due to its transparency in this region allows for easy detection of defects. MWIR of a plane, with a strong signal emitted from the high-temperature exhaust gasses. LWIR image of a soldier holding a rifle. FIR image of the Andromeda galaxy from the Herschel Space Observatory.

Since its discovery in 1800 by Sir W. Herschel, IR radiation has shown many unique properties, among which the possibility of seeing without an external source, and has found applications in many fields like astronomy, geology, biology, food industry and telecommunications. The high interest for this region of the light spectrum derives from the fact that this is where the EM radiation emitted by an object due to its temperature (also known as blackbody radiation) prevails over the light reflected from external sources, enabling applications like night vision, thermal and industrial imaging. The first IR sensors, dating back to the 1950s were mostly based on led chalcogenides (PbS, PbSe), a class of materials whose wide bandgap makes thermal detection suboptimal. Among the materials investigated in the following years, thanks to the technological advancements in semiconductor processing, III-V semiconductors, and specifically indium antimonide (InSb) appeared to be the best suited candidate for MWIR detection. However, by looking at the emission peak of a black body, whose spectral radiance can be calculated through Plank's law (Figure 2), one immediately finds that the emission peak of a body at room temperature occurs for values of wavelength around 10 μm. This result is further confirmed by Wien's displacement law, which can be used to find the value of the exact position of the peak:

$$\lambda_{peak} = \frac{b}{T}$$

where b = 2898 μm·K is a proportionality factor called *Wien's displacement constant*. It's easy to see that the emission peak of a body at 300 K is around λ = 10 μm, meaning that for thermal imaging, the range maximizing the photon flux is the LWIR. It's worth noticing that the left tail of the Plank's law curve is very steep, meaning that the intensity of emission quickly decays when moving away from the peak wavelength. This is beneficial for the fabrication of IR detectors, which will show a high contrast for signals emitted by bodies at different temperatures.

Further improvements in the semiconductor industry led to the development of narrow-gap semiconductors (InAsSb, HgCdTe and the less popular PbSnTe) during the 60s, enabling detection up to 15 μm. Less than 20 years later, owing to progress in the thin film growth processes, quantum well infrared photodetectors (QWIPs) were introduced; QWIPs are based on heterostructures between III-V

alloys (GaAs/AlGaAs was the first one). By carefully choosing the Al content, the stack of such layers forms a type I band alignment, resulting in quantum well formation if the GaAs width is limited to a few nm. This technology presents many benefits with respect to older ones, with faster response, improved thermal stability, homogeneity and yield (thus lower costs) thanks to the optimized wafer-scale fabrication. However, it suffers from being blind in normal incidence due to selection rules, requiring further introduction of light coupling gratings, and also from a relatively large dak current.

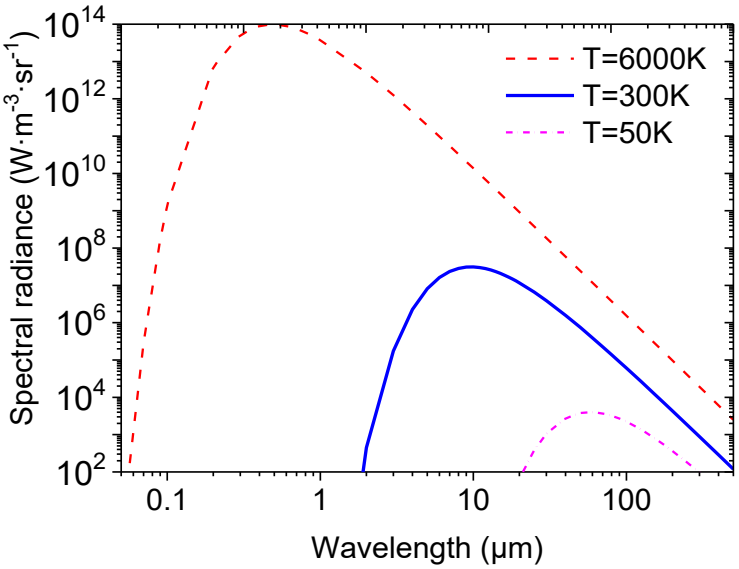

Figure 2: spectral radiance peaks for a black body at a temperature of 6000 K (dashed red curve), 300 K (solid blue curve), and 50 K (dotted pink curve). The maximum of intensity falls in the VIS, MWIR and FIR respectively.

Despite the numerous advantages, detectors based on bulk semiconductor alloys are fabricated through epitaxy; epitaxial growth is a complicated and high energy demanding technique which requires for expensive machinery. Moreover, epitaxial growth starts from costly single-crystalline and lattice-matched substrates: CdZnTe is used for the growth of HgCdTe alloy and its cost is above 1000$ per cm^2, and suffers from a high Cd content, which actually appears as the main source of heavy metal, far beyond the active layer. Lastly the integration between the final device and the silicon readout circuits (ROICs) is realized via flip-bonding, a complex and time-consuming technique. For these reasons today IR sensing is pricey and remains mostly limited to military and astronomy applications.

2.2 The mid-wave infrared

The MWIR region coincides with one of the transparency windows of Earth's atmosphere, meaning that photons with wavelength within 3 to 5 μm can travel in air with a very small chance of being absorbed. A further subdivision of this range into blue and red MWIR is possible when considering wavelengths below and above 4.26 μm respectively, this being one of the stronger absorption bands of CO_2. Sensing in the blue-MWIR is primarily addressed by XBn-InAsSb detectors [2], while for the red-MWIR Mercury Cadmium Telluride (HgCdTe, or MCT) detectors are commonly employed.

Together with the LWIR, the mid-wave band is also known as the "thermal infrared" since here is where objects with a temperature near ambience emit most of their thermal radiation. Due to these reasons, the applications for MWIR sensor are many and involve different fields:

- **Astronomy:** free-space communication and astronomical observation benefit immensely from the atmospheric transparency window, allowing data transmission with minimal losses. It's worth noticing that NASA's James Webb space telescope mounts MCT detectors for NIR detection, as well as Arsenic doped Silicon (Si:As) detectors for sensing in the MWIR, enabling wide-range imaging from 0.6 to 28 μm.
- **Military:** night vision and automated tracking rely on the signal emitted by hot bodies, which for jet plane or missile exhaust is maximum in this region.
- **Sensing:** high-sensitivity non-contact temperature sensing is enabled by the detection of MWIR photons. Gas sensing is also possible since many gaseous molecules (H_2O, CO_2, N_2O, CH_4) exhibit absorption edges in this region.

If we consider the energy range of photons in the MWIR (roughly 250 meV at 5 μm), it's easy to see how thermal excitation at room temperature (k_bT = 25 meV) is just 10 times smaller than energies in the range of interest. The activation of charge carriers toward the excited state is a competition between photon and phono activation, where the latter is the main limiting factor for the signal-to-noise ratio (SNR), and is known as *dark current*. For this reason, MWIR detectors are commonly operated at cryogenic temperatures in order to minimize thermal noise. This allows to increase the SNR and to reach the maximum values of resolution and sensitivity. The lower the temperature of operation, the easier the detection of objects against a background at a temperature which is close to theirs.

2.3 Colloidal quantum dots (CQDs)

For the past 40 years, a new class of materials emerged as the possible successor to bulk III-V semiconductors for the assessment of IR applications: colloidal nanocrystals. CQDs consist of a nanometric semiconductor core, whose surface is covered by branched molecules, called *ligands*. Many semiconductors can be synthetized under the form of nanocrystallites (CdSe, HgTe, PbS just to mention a few), while the most utilized ligands are organic molecules whose length separates them into two categories:

- **Long ligands:** oleic acid, trioctylphosphine oxide, dodecanethiol are a few examples. These molecules consist of a long carbon chain (e.g., 18 carbon atoms, for a total length at around 2 nm) and are used for synthesis, conferring colloidal stability to the solution, and passivating the surface of the nanocrystals.
- **Short ligands:** this class includes ethanedithiol, mercaptopropionic acid and ethylenediamine. Their shorter carbon chain is used to improve the transport properties of CQD films.

As the name suggests, these nanometric semiconductor solids can be synthetized in solution, conferring them the advantage of being easily mass produced.

2.3.1 CQD synthesis

The colloidal synthesis of semiconductor quantum dots began in the early 1980s, driven by the interest in obtaining better performing solar cells, exploiting the more efficient multiple exciton generation in confined systems. A major milestone for this field arrived in 1993 with the *hot injection* method by the Bawendi group at the Massachusetts Institute of Technology, which earned him the 2023 Nobel prize in chemistry, alongside Brus and Ekimov, for the discovery and synthesis of quantum dots [1,3,4]. The relevance of this synthesis methodology stems from the possibility of obtaining monodispersed (i.e., atom like) CQDs, of controllable size and shape, using the equipment one can find under a standard fume hood found in most chemistry labs. This procedure begins with the rapid injection of precursors into a hot solvent. Concerning the precursors, the cation is dissolved in a mixture of solvent and ligands, used to slow down the growth kinetic and maintain nm size. They also later ensure the colloidal stability of the particles while also passivating the surface dangling bonds. The mixture is first degassed to remove water

and oxygen that may later oxidize the formed semiconductor. Then the temperature is raised under a neutral gas and the size and shape of the NCs is tuned by the control of the growth parameters, like temperature, time and by the choice of ligands in the solution. The monodispersity of the final QDs is essential to obtain devices with a sharp absorption edge.

In modern days colloidal nanocrystal synthesis has reached the industrial production scale, mainly for the fabrication of displays, which use core-shell quantum dots technology. The latter allow for the passivation of surface defects in bare NCs, that act as non-radiative recombination centers. Core-shell QDs are exploited for their sharp emission lines, conferring them the ability of producing colors of high purity, and for their higher efficiency in light conversion, which reduces energy consumption.

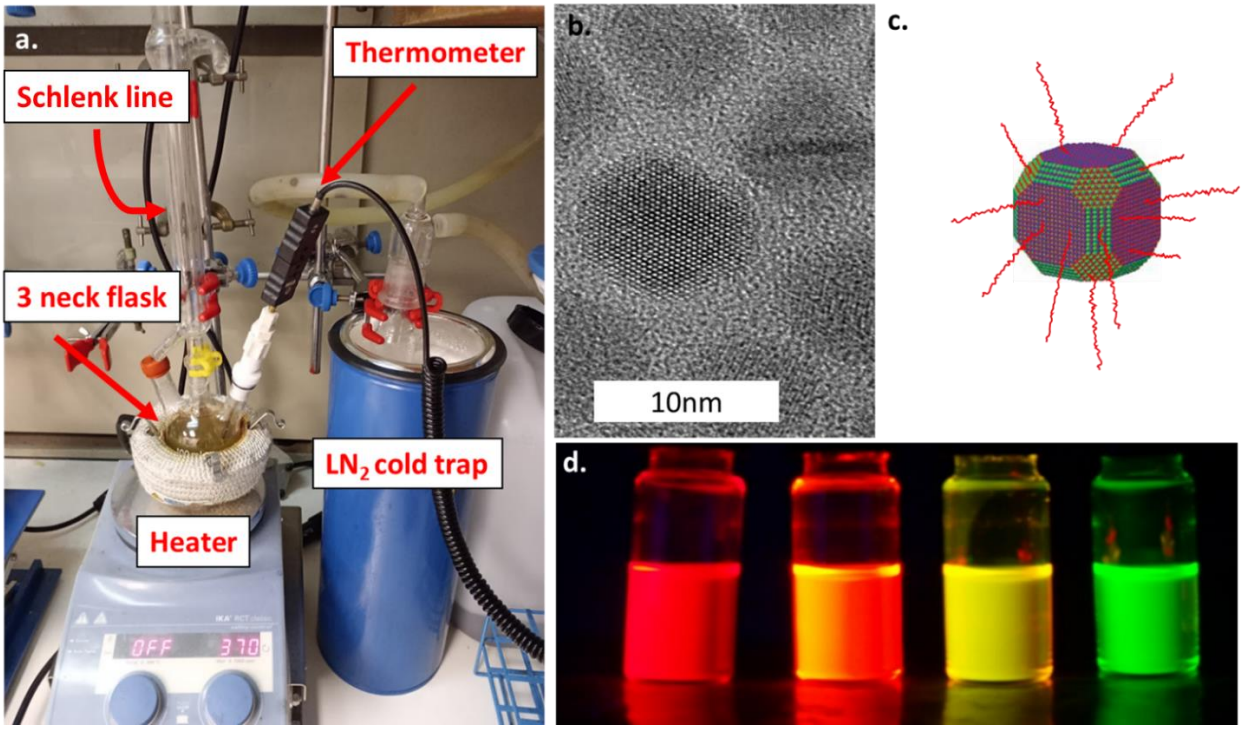

Figure 3: a. Experimental setup for the synthesis of CQDs, following the hot injection method. b. Transmission electron microscope (TEM) image of PbSe nanocrystals. c. Illustration of a nanocrystal core (PbS) capped with ligands. d; Emission from CdSe CQDs of different sizes when illuminated by ultraviolet light.

2.3.2 Quantum confinement

When the size of a material approaches the Bohr radius (7 nm for CdSe, 40 nm for HgTe [5]), quantum confinement induces a discretization of the energy spectrum. This non-classical phenomenon, caused by the increase of the effective bandgap when the dimensions of a material approach the nanometer scale, changes the electronic and optical properties of the material itself.

If we take the case of a spherical nanocrystal of radius R, we have that the energy of an electron in the conduction band, due to quantum confinement, is discretized. For most semiconductors the electron (hole) energy near the center of the Brillouin zone is

$$E_i \approx E_{c(v)} + \frac{\pi^2 \hbar^2}{2m_{e(h)}R^2}$$

When a photon is absorbed by the semiconductor, an electron will be excited to the conduction band leaving a hole in the valence band; the two carriers, having opposite charge will be attracted by Coulomb interaction, forming a bounded state called exciton. By considering this interaction, the optical bandgap can be defined as:

$$E^* \approx E_g + \frac{\pi^2 \hbar^2}{2m_{eh}R^2} - \frac{1.8e^2}{\varepsilon_r R}$$

where E_g is the bandgap op the bulk material, and $m_{eh}^{-1} = m_e^{-1} + m_h^{-1}$ is the reduced effective mass. From the last equation we see that the second and third contributions have opposite sign: the confinement term tends to increase the value of the optical bandgap as the size is reduced, while the Coulombic term has the opposite effect. Since the radius of the crystallite appears to the second power in the confinement term, the increase of E^* when shrinking the nanoparticle. Moreover, the weakness of the attractive term with respect to the confinement energy, causes the generated pair to be localized primarily due to the confinement potential rather than their reciprocal attraction.

Considering the case of HgTe (see Figure 4), which in its bulk form is a semimetal (i.e., $E_g = 0$), we immediately see how the optical bandgap can be tuned over a wide spectral range if one is able to control the size of the nanocrystals. This means that the absorption of HgTe NCs can range from virtually zero for very large crystals, to up to 1.5 eV for the most confined form, making them one of the most versatile materials available for detection from the NIR up to the LWIR potentially. The large spectral tunability of HgTe CQDs, alongside with the silicon-compatibility, the possibility of being spin casted directly on focal plane arrays (FPAs) [6], the solution processability and the possibility of functionalizing the surface of the nanocrystals is what made this material so appealing to researchers over the last decades.

2.3.3 HgTe nanocrystals

Conventional wide bandgap semiconductors, such as cadmium chalcogenides (CdSe, CdTe), show absorption in the visible range. These materials, like most semiconductors, exhibit a normal band ordering at the Γ point. The conduction band (CB), characterized by Γ_6 symmetry, is mostly composed of the Cd s orbitals, while the valence band (VB), with Γ_8 symmetry and composed mainly by the p orbitals of the chalcogen, has lower energy. The VB is 8-fold degenerate, while the CB presents weaker (2-fold) degeneracy, while being much more dispersive, leading to a lower effective mass for electrons. Finally, the split-off band, originated from the spin-orbit interaction, is located in the valence band, and causes the splitting between light hole (LH) and heavy hole (HH) bands. The band structure for mercury chalcogenides shows a completely different picture. In HgTe the band with Γ_6 symmetry is has lower energy than the one with Γ_8 symmetry, or in other words it shows an *inverted band ordering.* Due to this, the CB in HgTe has the same symmetry of LH band in CdSe.

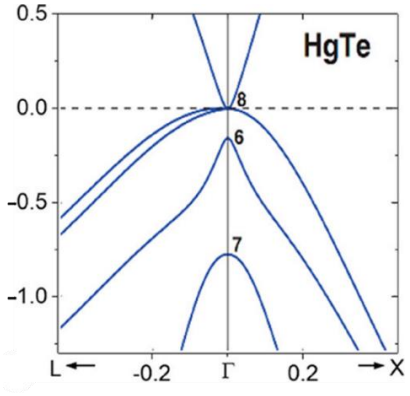

Figure 4: Band structure near the Γ point of HgTe, obtained from a hybrid QSGW approach, from ref. [7] . The unit along the x axis is 2π/a, with a = 0.647 nm.

As shown in Figure 4, the strong dispersion in the CB of HgTe leads to an electronic effective mass which is very low (0.01 – 0.03 m_0), which reflects into a very high bulk carrier mobility (greater than 1000 $cm^2V^{-1}s^{-1}$ at room temperature) for electrons. The opposite occurs for the VB, whose weak dispersion reflects to a greater hole mas, which is larger than 0.3 m_0. The Fermi level in intrinsic bulk HgTe is located

between LH and HH bands, which at the Γ point share the same energy, making this material a semimetal. This property has an extremely important impact on the optoelectronic properties of HgTe CQDs, whose spectral tunability is not limited by the bandgap in the bulk material.

Optical absorption occurs when a photon is absorbed by a material, transferring its energy to an electron, who is excited from a filled ground state to an empty excited state. In HgTe the initial state is located in the valence band with HH symmetry, while the excited one is in the CB with light hole symmetry. When we focus our attention on nanocrystals of the same material, quantum confinement raises two novel properties:

- **Discretization of the density of states:** quantum dots are solids whose dimensions are confined both in the x, y and z direction, causing the density of states to be described by a series of broadened delta functions.
- **Bandgap opening:** as shown in Fig. 4, when the size of the material is isotropically reduced to a few nanometers, states at the center of the Brillouin zone are no longer available, causing the appearance of an effective bandgap. Since the bulk bandgap in HgTe is null, the magnitude of this effective, or optical bandgap will depend solely on the entity of the confinement, i.e., on the dimension of the NCs.

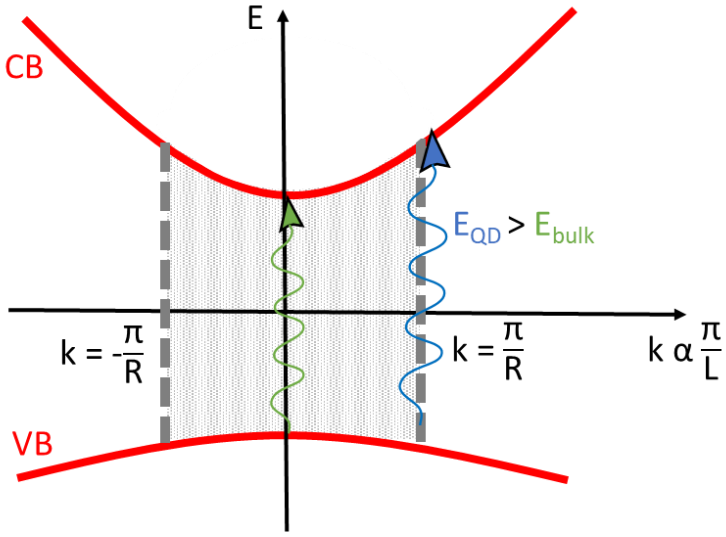

Figure 5: Effect of wavevector quantization on the optical bandgap of a semiconductor. The grey shadowed area becomes inaccessible due to the nanometric dimension of the system, thus the transition depicted in green is no longer allowed.

In order to obtain sensing devices out of HgTe CQDs, the long ligands that cover the surface of each crystal to ensure the colloidal stability of the solution, need to be replaced by shorter ones, with the purpose of increasing the density and conductivity of the film that will be used as active area of the device. This process is called *ligand exchange* and it is usually implemented following one of two possible alternatives:

- **Solid-state ligand exchange:** this technique consists in exposing a film of NCs capped by long ligands to a diluted solution containing shorter ones, usually by dipping the sample in the solution itself. This technique is not ideal when working with thick films, as only the QDs closer to the surface of the film will be exposed to the short ligands. Moreover, as the ligand exchange occurs, the volume of the film tends to shrink, leaving voids and cracks detrimental for conduction. This process can be iterated multiple times to obtain thicker films and heal the defects introduced by ligand exchange, with the drawback of increasing the probabilities of flaking and delamination to occur.

- **Liquid phase ligand exchange:** this more recently developed technique was introduced with the aim of solving the poor film quality caused by solid state ligand exchange[8]. This consists in creating a colloidal dispersion based on short ligands which are transport-compatible. To achieve liquid phase exchange, a solution of a polar solvent and short ligands is mixed with the long-ligands capped QDs dispersed in a nonpolar solvent. The polar phase containing the short ligands NCs will separate from the nonpolar one containing the long ligands, which can be discarded using a pipet.

After liquid phase ligand exchange is performed, the colloidal dispersion containing the QDs is twice before precipitating, drying and finally redispersing the NCs in dimethylformamide (DMF). These final steps allow to obtain a solution which can be drop-casted or spin-coated to obtain conductive films, able to achieve mobilities up to 100 $cm^2V^{-1}s^{-1}$ for the record value, and in the 0.1 to 1 $cm^2V^{-1}s^{-1}$ range for more conventional value. This nevertheless contrasts with initial value for pristine film with mobilities below 10^{-6} $cm^2V^{-1}s^{-1}$ [9].

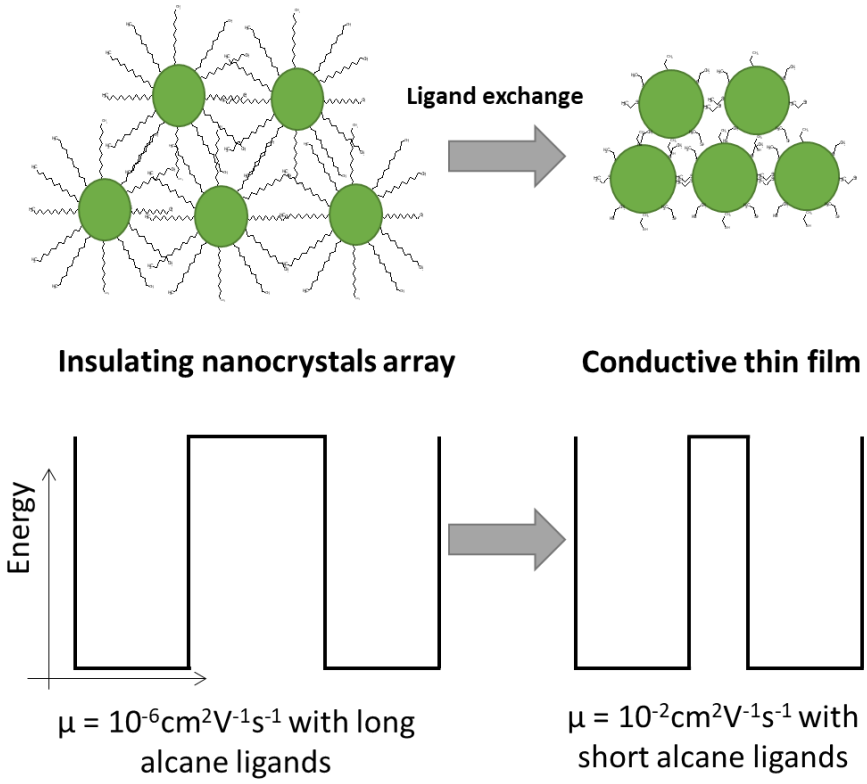

Figure 6: illustration showing the effect of ligand exchange, shorter ligands constitute a thinner barrier for hopping.

Ideally, after synthesis and ligand exchange the NCs are monodisperse (they are characterized by the same composition, size and shape), and the surface of each crystal presents the same distribution of ligands. During spin coating, microbubbles and pinholes may form on the film, which from a transport standpoint act as energy barriers. These imperfections reflect into an energy landscape which is not uniform, owing to localized and weakly coupled electron and hole states between neighboring crystals. For this reason, when an electric field is applied to the NCs film, carriers whose energy is high enough to overcome the energy barrier constituted by the ligands, will hop to an adjacent state toward the electrode, in what is known as *hopping transport*. In this regime, transport is enabled either by thermal excitation, conferring charge carriers enough energy to overcome the barrier, or by quantum tunnelling through the barrier. The hopping mobility is given by [10]:

$$\mu_{hop} = \frac{ed^2 E_a}{3hk_B T} e^{-\beta w - E_a/k_B T}$$

where e is the elementary charge unit, d is the distance between the centers of the particles, E_a is the hopping activation energy, h is Plank's constant, β is the attenuation of the wave function probability in the barrier, w is the barrier width, k_B is the Boltzmann constant, and T is the temperature of the system. It's evident how the mobility in a nanocrystal film strongly depends on the barrier thickness, which is directly related to the length of the ligands, hence the need for ligand exchange before the spin coating of the CQDs solution.

Over the last few years, MWIR detectors based on CQDs have reached performances which are comparable to commercially available products, with values of detectivity up to high 10^{10} Jones for photoconductors, and $7x10^{11}$ Jones (T_{op} = 80 K, λ_{cutoff} = 5 μm) for cryocooled photodiodes[11]. Current research is aimed at improving the design of these devices to enhance their performance, exploiting for example photonic phenomena like cavity resonances or surface plasmon polaritons, replacing standard materials such as gold electrodes with more sophisticated ones as graphene, and by finding ways to improve the stability of the NCs with core-shell structures.

3 Internship subject: MWIR detectors based on HgTe nanocrystals

My internship revolved around the employment of mercury telluride nanocrystals for the fabrication of devices for sensing in the mid-wave infrared. This chapter is divided into three subsections, over which I introduce the different technologies available for infrared detection with nanocrystals, as well as the commercially available alternatives, their flaws, and the reason why we believe that CQDs could be valid substitutes. This chapter ends with a section dedicated to the objectives of my work inside of INSP.

3.1 Infrared detection

The maturity that HgTe CQDs have reached over the last decade has raised interest in the scientific community in the exploration of their possible employment both as absorbers and emitters. The first sensing devices, due to the simplicity in their fabrication, were photoconductive.

A photoconductor (PC) based on CQDs is simply a film of nanocrystals deposited between two electrodes. The thickness of the film should be carefully addressed because of the tradeoff that is inevitably met between charge transport and photon absorption. In order to optimize charge collection from the electrodes, thin films are desirable to avoid photogenerated carriers to be recombined onto the numerous trap state generated at the surface of this highly defective film. However, a film which is too thin is detrimental both in terms of light absorption, since less material translates directly to a lower probability of a photon to be absorbed, and on the transport side, a film which is too thin would lead to 2D hopping transport, causing a drop in charge carrier mobility because of the reduced coupling between states in neighboring quantum dots.

During the development of photoconductive sensors, a huge improvement in the performance came from substituting standard gold contacts with interdigitated electrodes (IDEs). These consist of two electrodes casted in the shape of two comb-like arrays of interleaved conductive strips, which do not touch each other (Figure 7). This particular pattern allows for an improvement of detector performance in two ways:

- Amplification of charge collection by increasing enormously the surface that is available for collection. Moreover, a nonlinear electrode shape allows for a better collection of a round shaped light beam.

- Reduction of the overall resistance of the device, due to the increase in contact area between CQDs and electrodes. This allows for an easier measurement of electrical properties.

These electrodes can be lithographically patterned on substrates like glass or silicon (which do not impose any constraints related to epitaxy), and successively coated with NC films by either spin coating, drop casting, spray coating or imprinting, among other available techniques. Photoconductive detectors can nowadays reach high values of detectivity, while exhibiting fast responses down to few ns. They nevertheless suffer from a large dark current due to the need to apply an electric field to collect the charge and dissociate the electron hole pair.

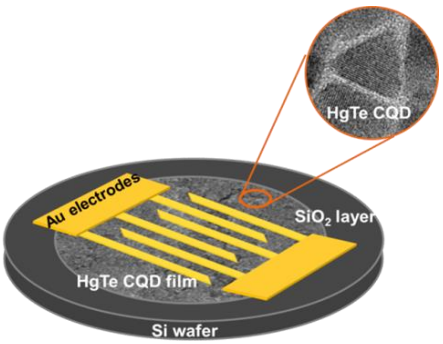

Figure 7: illustration of the typical layout of a photoconductor, constituted by gold interdigitated electrodes (in yellow) deposited on a SiO_2/Si substrate (gray disk), and covered by a thin film of HgTe CQDs. The NC film represents the active area of the device, dedicated to the absorption of light and production of charge carriers, which are collected by the electrodes upon the activation of an electric film between them. From ref. [12].

Another strategy to reduce the high dark current that characterizes photoconductors, is through the exploitation of the gate effect. When a voltage is applied to a CQD film through a dielectric, the Fermi level inside of the film can be shifted. This shift can be used to balance the doping of NCs in the film, bringing the Fermi level of the system to the middle of the bandgap. When this happens, the energy required for electrons be promoted to the conduction band is maximum, and the dark current will be minimized.

One of the other uses for field effect transistors (FETs) is to probe the transport properties of the devices. FETs include three electrodes: source (S), drain (D) and gate (G): the drain bias is used to accelerate the particles, while the gate is in charge of tuning the carrier density. When a positive bias is applied between the first two contacts ($V_{DS} > 0$), a current will be drawn from source to drain, through the material of interest, which in our case is HgTe NCs. Different materials can be used for the gate (dielectrics, ferroelectrics, electrolytes), and depending on what is chosen, two types of FET geometries are used in our group:

- **Back-gate FET:** an illustration of the typical configuration of these devices is shown in Figure 8 a. The dielectric material is commonly an insulating oxide (SiO_2, Al_2O_3). When a positive bias is applied to the conducting layer below the dielectric ($V_{GS} > 0$), positive charges accumulate at the interface between the insulating layer and the NCs, causing an injection of electrons in the film to compensate for this unbalance.
- **Top-gate FET:** shown in Figure 8 b. This configuration uses an ion-gel electrolyte, such as lithium perchlorate ($LiClO_4$), on top of which a copper grid is placed, to allow for a uniform distribution of the electric field inside of the gate medium. When a $V_{GS} > 0$ is applied, Li^+ ions will percolate within the NC film, and as in the back-gate case, an injection of electrons from the contacts is needed to balance the positive charges.

The advantage in using electrolytes as gate media is that thanks to their higher gate capacitance (around 1 μF cm^{-2}, vs 1 nF cm^{-2} of gate oxides), a strong modulation of the carrier concentration can be obtained with relatively low biases. Furthermore, electrolytes are better for the gating of thick NC films, thanks to the diffusion of ions inside of the active layer. The main drawback of this technology is that being based on ion displacement, which is intrinsically slow, it will limit the gate bias sweeping rate, since a longer time will be required for a steady-state condition to be reached when a V_{GS} is applied. Furthermore, the ion- gel electrolytes must be operated above their freezing temperature, which is well above the normal operating temperature of IR detectors. It should be mentioned that gate voltages should not be too high, because of the low electrochemical stability of these compounds.

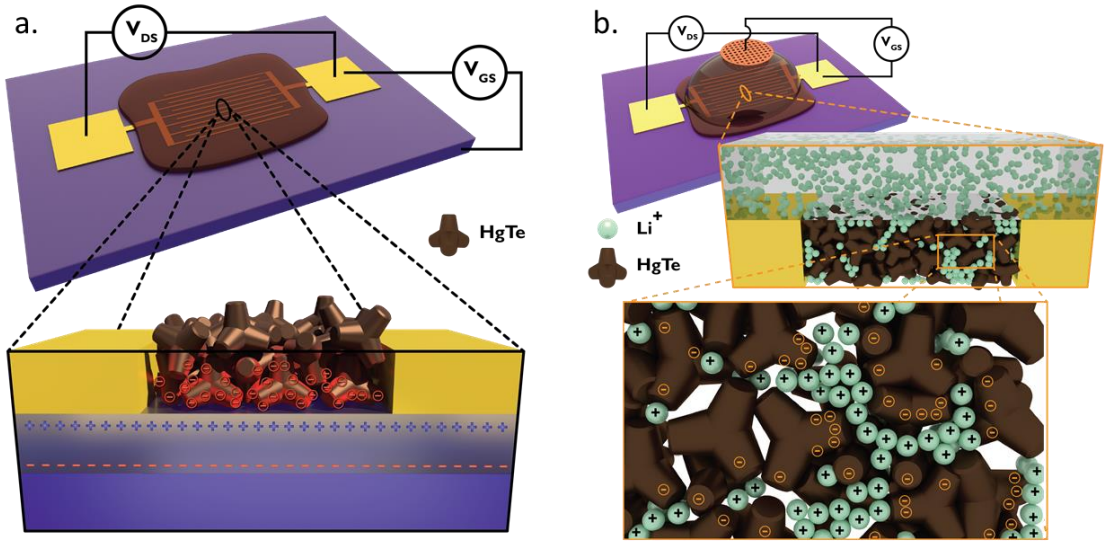

Figure 8: a. illustration of a "back-gate" FET, in which SiO_2 is the gate dielectric. b. illustration of a "top gate" FET, where the gate material is a $LiClO_4$ ion-gel electrolyte. From ref. [13].

Independently on the configuration of choice, FETs are used to probe transport properties, like the mobility of carriers in the semiconducting film. This is done with the acquisition of a *transfer curve*. When a constant bias is applied between drain and source, the current will depend on the gate bias, with which conductivity modulation is carried out. Depending on the behavior of the current when a positive or negative gate bias is applied, two types of semiconductors can be distinguished: p type or n type. In a p-type semiconductors, holes are the majority carriers, i.e., those with a higher concentration in the material, which will thus give a higher contribution to the formation of a current. A p-type material will exhibit an increased I_{DS} when a negative bias is applied (a negative bias will shift the Fermi level towards the valence band, increasing the density of holes). On the other hand, if a current increase appears for positive gate bias, the majority carriers in the material are electrons, and the semiconductor is called n-type. When the material shows both type of behaviors, it is referred to as *ambipolar.*

When V_{DS} is small compared to V_{GS}, the concentration of carriers can be assumed to be uniform along the channel, and the carrier mobilities are given by:

$$\mu = \frac{L}{W C_i V_{DS}} \cdot \frac{\partial I_{DS}}{\partial V_{GS}}\Big|_{V_{DS}}$$

where L is the length of the channel, W its width, C_i the sheet capacitance of the gate insulator, and the derivative of the drain-source current has to be calculated under constant V_{DS}.

The choice of the gate material is crucial for device performance, and the use of ionic glasses like LaF_3 can provide high capacitances at low temperatures, as well as a tool for the control of the photoresponse[13].

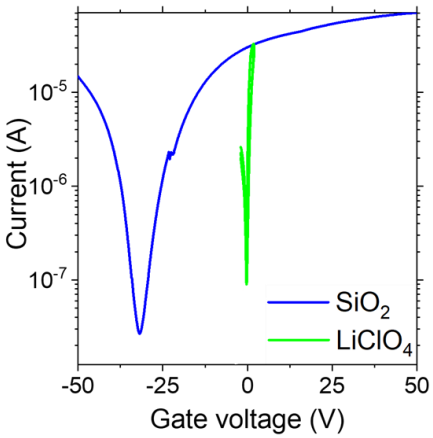

Figure 9: transfer curves for a HgTe phototransistor with different gate materials: SiO_2 in blue and $LiClO_4$ ion-gel electrolyte in green. As shown, the electrolyte is able to give a modulation of I_{DS} of over 2 orders of magnitude, despite the V_{GS} is much smaller. From ref. [13].

One last alternative route for detection with CQDs is that of photodiodes. The lower noise current when under photovoltaic (PV) operation is one of the benefits coming from the higher complexity of these devices. Two alternatives are currently available for the fabrication of HgTe photodiodes:

- **Vertical diode stacks:** These devices consist of a layer of CQDs sandwiched between two contacts, used for charge extraction (Figure 10). Electron and hole transport layers are commonly added to the stack for a more efficient collection of charge carriers, ensuring a better band alignment, and blocking the transport of minority carriers toward the electrodes. In particular, transparent conductive oxides are used as transport layers for electrons, and concerning holes, a layer of Ag_2Te NCs is commonly employed [14]. The problem with this solution is that the spatial inhomogeneity and diffusion uncontrollability of the Ag^+ ions result in response nonuniformity, other than the difficulty in the subsequent deposition of different CQD films, which often lead to delamination.
- **Lateral diodes:** recently proposed electric field-activated doping process have allowed the group of Qin to obtain lateral p-n junctions in which the doping level can be spatially adjusted through the polarity and activation time of the electric field which is applied to the NC film[15]. This device operated in PV mode was able to obtain an improvement of one order of magnitude in detectivity with respect to the same one operated in PC mode, other than an improvement in response speed from millisecond to microsecond.

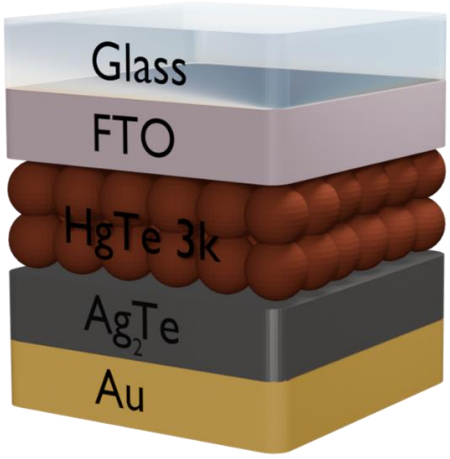

Figure 10: illustration of a vertical stack diode. The HgTe active layer is sandwiched between two transport layers, Ag_2Te for holes, while FTO acts both as an electrode and an electron transport layer.

Photodiodes consist today the best performing detectors, reaching detectivities in the SWIR up to 9×10^{11} Jones at temperatures of 200 K [16]. Improvements on diode performance can be achieved with the integration of photonic structures to exploit resonances and enhance electric fields, for example replacing the conductive oxide electrodes with carefully designed metallic gratings [11,17].

3.2 State of the art mid-wave and long-wave infrared detectors

Commercially available IR imagers with the best performances are based on bulk MCT. This technology presents an extremely wide spectral tunability, from the SWIR to the LWIR, which can be addressed by adjusting the ratio of mercury to cadmium in the material. This ternary alloy is a combination of two binary semiconductors, cadmium telluride (CdTe) and HgTe, and its general formula is $Hg_{1-x}Cd_xTe$. The ratio of Cd in the alloy (x) can be tailored to obtain the desired value of the bandgap to address a specific IR region. This makes MCT the only commercially available material that can detect IR radiation in both of the available atmospheric windows, the 3-5 μm window in the MWIR range, and the 8-12 μm window in the LWIR. The popularity of this material also stems from two other fundamental qualities: its excellent sensitivity, which stems from the impressive external quantum efficiency (which can reach values of up to 80% for MWIR and 70% for LWIR detectors). The other quality that makes MCT detectors so sought after is the good time response, property which is particularly appreciated in military application, where the objects of interest can be fast-moving.

Despite its many qualities, handling MCT comes with several challenges that limit the potential applications of this material. First of all, HgCdTe is grown using Liquid Phase Epitaxy (LPE), a very complex process during which a substrate is dipped into a very hot growth solution containing the epitaxial material. By carefully controlling the temperature, supersaturation can be reached, causing the crystallization of the material of interest onto the substrate. This technique is highly demanding from the energetic standpoint, and it requires expensive control systems to carefully tune the growth parameters, such as temperature, melt composition and growth rate, to obtain a good quality result with minimal dislocations. These are crystalline defects that act as recombination centers for charge carriers, they are thus detrimental for the performance of the final product, and to reduce their occurrence, expensive lattice-matched substrates like cadmium zinc telluride (CdZnTe) are used. CdZnTe is a costly material which is difficult to fabricate in large sizes, and even when this substrate is used, threading dislocations can propagate to the MCT epilayer, reducing the sensitivity of the final detector while also increasing the noise. When the bulk MCT is grown, the typical semiconductor processing (lithography, etching, doping, metallization and passivation) is carried out, to obtain a detector array with the specific characteristics (spectral response, operating temperature range, shelf life) that the manufacturer is aiming for. After that, the focal plane array (FPA) is hybridized with a readout integrated circuit (ROIC), usually made of silicon, using bonding techniques like the flip-chip bonding. Flip-chip bonding is what limits the pixel size in MCT devices to the micrometer range (typically 10-15 μm), due to the complicated control over bump size, bump pitch, and difficulties in alignment as the pixel sized is reduced.

When talking about state-of-the-art sensors in the blue MWIR, one must mention detectors based on type 2 heterostructures like InAs/GaSb [2]. These devices, also known as barrier diodes, use a barrier and an active layer which have the same doping, in order to exclude the depletion region from the absorbing layer. This is done to reduce the effect of generation-recombination currents by a factor 100, which in turn allows for a relaxation on the requirement of low operating temperature that normally affects quantum well infrared photodetectors (QWIPs). These devices rely on intersubband transitions to detect IR radiation, between minibands whose position in energy can be controlled by tuning the parameter of the well (height, which depends on the material of choice, and width). The advantage in using these materials is that they do not need expensive substrates to initialize the growth, and their fabrication does not involve toxic heavy metals like mercury or cadmium.

3.3 Objectives

The objectives of my internship are to gain confidence with the process of fabrication and characterization of detectors based on mercury telluride colloidal quantum dots. This includes being able to fabricate a device starting from the bare substrate in a cleanroom environment. The fabrication process includes substrate preparation and deposition of thin metal layers using the lift-off method, which I will explain in further detail in the following chapter. For this purpose, I needed to be familiar with the routine procedures to access the cleanroom, and to learn how to operate machinery such as the mask aligner and the evaporator, which are the two most important tools needed during a lithographic process. I also trained in the synthesis of colloidal quantum dots, and in their processing to prepare a NC solution which can be spin coated, to produce a film which is photoresponsive and conductive. This work allowed me to understand the difficulties in the procedure to optimize a recipe for the production of a stable CQD solution. For the production of good quality films, I used spin coaters and a mechanical profilometer, which is a machine that uses a stylus brought to contact with the surface of interest to gain information on its roughness.

During the last day at INSP, I was involved in the fabrication of CQD based vertical stack diodes. These layered structures require multiple deposition steps, some of which were carried out inside of a glovebox. The latter is a controlled environment, commonly used for the processing of easily oxidized materials. During the fabrication of diodes, the deposition of Ag_2Te was carried out in a glovebox.

Once the detector was successfully fabricated, I started working on its characterization, in order to determine the performance both in term of optical absorption, and of electrical conduction. This process required me to learn how to mount samples in a cryostat, needed for the low temperature measurements. Electrical connections allow to connect the sample inside the cold head to the instrumentation for the electrical characterization (multimeters, lock in amplifiers, and noise spectrometers). For the experiments requiring the generation of a photocurrent, I was shown how to use photon sources like lasers at different wavelengths (such as the quantum cascade laser and the 1.55 μm telecom wavelength laser) and the blackbody radiation source, useful for the possibility of reproducing the emission of a hot object at different temperatures. In order to gain information on the spectral characteristics of the devices, I used a Fourier transform infrared spectrometer (FTIR). The latter is used to characterize both the absorption of the material and the photoresponse of the device. During characterization, the most important quantities that I was interested in obtaining were external quantum efficiency (EQE), the specific detectivity (i.e., signal to noise ratio), the spectral response and dark current, which are the most relevant figures of merit to determine the quality of a photodetector.

4 Results

My project is focused on nanocrystal based mid-wave infrared sensors. This chapter is divided in two sections, one dealing with the typical workflow for the production of a CQDs based detector, and the second treating the most important parameters and the techniques to obtain them.

4.1 Sample fabrication

The first part of the project has been focused on photoconductors and phototransistors geometries. These devices consist of a few hundred nanometers thick NCs film deposited on gold electrodes. In the following sections the typical steps to obtain a working single pixel device are shown.

4.1.1 Deposition of gold electrodes

The devices are fabricated starting from gold interdigitated electrodes deposited on various substrates, such as glass, silica, or dry silicon oxide grown on top of silicon for the realization of "bottom gate field effect transistors.

Substrates are first sliced using diamond tip to match the targeted pattern size, and at the same time maximize the number of samples that can be fitted inside of the evaporator for the deposition of the metal layer. After slicing, the substrate is covered in dust particles that are removed using an acetone flow. Cleaning begins by submerging the substrates into an acetone bath and sonicating it for a few minutes. This ensures the removal of organic matter. The samples are then removed from the acetone bath and rinsed with acetone and isopropanol (IPA), used to wash away any residue of acetone. Finally, the substrate is dried with N_2 gas and further cleaned using O_2 plasma, to ensure the effective removal of any microscopic contaminants, and to activate the surface by making it more reactive, with the purpose of improving adhesion of the photoresist primer.

When working with silicon or glass, a primer is spin coated on the substrate to improve the bonding between the photoresist (PR) layer and the substrate. This step, which may seem trivial, is critical to obtain a successful lift-off. Once the surface is primed, the PR can be deposited. A photoresist is a solution made of three components: a solvent, a polymer base, and a photoactive compound (PAC). When energy is transferred to the PAC, usually under the form of UV light, the polymer base is made more or less soluble, depending on whether the resist is positive or negative, respectively. A third type of resist, called image reversal, allows to obtain features with a negative slope, which is extremely helpful during the lift off step. The PR I used during fabrication is the AZ5214E image reversals resist by MicroChemicals.

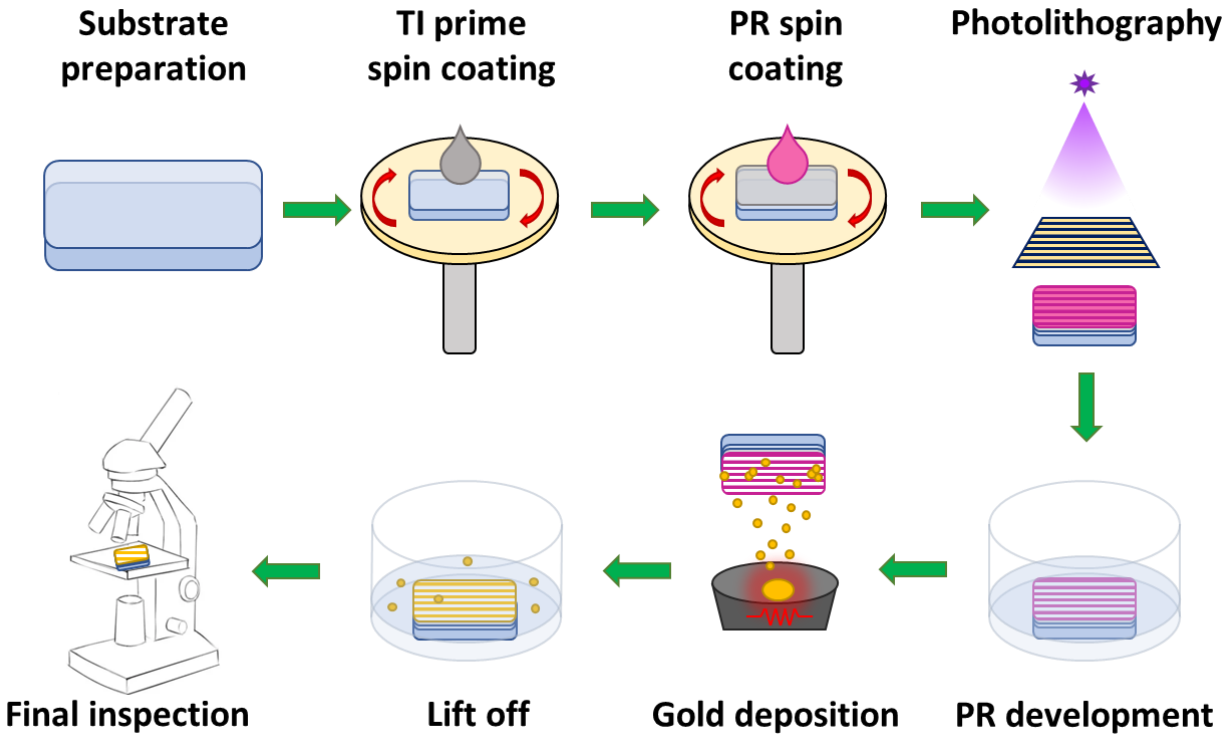

Figure 11: illustration showing the main steps in a lithographic process. Following the green arrow: start from the sliced and cleaned substrate. TI prime spin coating. PR spin coating. Patterning using UV light. PR development. Deposition of a thin film of gold. Lift-off to reveal the patterned electrodes. Final inspection and electrical testing.

Once the PR layer is deposited, the sample is transferred to the mask aligner. This machine is used to properly align the mask containing the pattern to be transferred to the photoresist layer. Ultraviolet (UV) masks consist of a quartz square-shaped slab covered by chromium. The chromium layer is used to reflect UV light and prevent the exposition of areas which should not be illuminated, and is patterned by more sophisticated techniques such as e-beam lithography. After alignment, mask and substrate are brough into contact, and the PR is exposed to UV light for 1.5 seconds. The substrate undergoes the reversal bake for 2 min at 125 °C on a hot plate and flood exposure (40 s exposure without mask), and after that the PR is ready to be developed. At this stage, before development, the desired pattern should be visible on the sample when observing it under grazing light, confirming that the exposure step was performed correctly.

Then the PR is developed by dipping it in a developer solution (i.e., usually an alkaline solution), for which I used the AZ726 by MicroChemicals. The duration of this step should not be critical as long as the previous steps, and in particular reversal baking, have been done properly. Here we use a typical duration at around 30s. The reaction is stopped by dipping the sample in a water bath.

At this point the surface of the glass substrate is bare where the final gold electrodes should be, and it's covered by photoresist elsewhere. In order to remove any residual resist from the areas that should be uncovered, and to promote the adhesion of metal in the following step, the samples undergo a 2 minutes plasma cleaning phase. After that, the samples are fixed to the sample holder of the evaporator using metal clips, to prevent them to move and/or fall once the sample holder is mounted upside down in the evaporator. The evaporator is a vacuum chamber in which alumina boats are filled with different metals. These metals are heated above their boiling point by Joule heating, and the metal atoms travel upward towards the substrates, where they condense. The sample holder is able to rotate in order to minimize shadowing effects and obtain a more uniform film. For my deposition, a thin layer (5 nm) of chromium was deposited to assist the adhesion of a thicker 80 nm gold layer.

The last step in the lithographic process is lift-off. This consists in submerging the samples in acetone to remove the residual photoresist with gold on top from the areas which should not be conductive. The plate containing the samples submerged in acetone should be gently agitated to help fresh solvent to come into contact with the photoresist. If the procedure results slow or difficult, placing the samples in an ultrasonic water bath (commonly referred to as "sonicator") for 5 minutes may help. When the procedure is complete, the surface of the sample is rinsed with acetone to remove any unwanted gold flakes that may be attached to the surface, then flushed with IPA and finally dried with a N_2 gun.

To ensure that the deposition is completed successfully, the channel between the electrodes can be observed under an optical microscope, and a multimeter can be used to verify that none of the contacts are short-circuited.

4.1.2 Nanocrystal synthesis

The HgTe nanocrystals are synthetized in colloidal solution following a scaled-up version of the Keuleyan's procedure[18]. This synthesis requires an advanced user, thus the NCs were always synthetized by Y. Prado, the group's chemist engineer.

I was personally involved in the synthesis of nanocrystals of a different binary compound semiconductor, which is led sulfide (PbS). Led chalcogenides such as PbS were the first materials used for the first IR sensors developed starting from the 1950s. The narrow bulk bandgap that characterizes these materials is the reason why they were limited to detection in the NIR and SWIR ranges. Under nanocrystal from, their growth have first been proposed by Hines et al [19], but here we used an alternative approach proposed by Moreels et al [20]. The chemicals used in the synthesis of PbS CQDs are safer, making the preparation more suited for a first experience with nanocrystals

For the synthesis of PbS nanocrystals, the following chemicals were utilized

- 300 mg $PbCl_2$
- 30 mg sulfur powder
- Oleylamine
- Solvents (toluene and hexane)

The synthesis is carried out under a fume hood to avoid exposure to volatile compounds that may be released during the process. The 50 mL 3-neck round bottom flask is connected to a Schlenck line, whose role is to provide either vacuum or neutral gas. A cold trap kept at liquid nitrogen temperature (77 K) is used for the condensation of gaseous byproducts to avoid them from reaching the pump. A heating mantle is used to heat up the solution during the process while a magnetic stirrer ensures homogenization of the solution, and a thermometer probe connected to a PID is inserted in one of the 3 necks of the flask to monitor the temperature.

The synthesis of PbS NCs in organic medium starts from combining the lead precursor ($PbCl_2$) into the flask together with 7.5 mL oleylamine (OLA) that act as both solvent and ligand, and heated to 85°C while stirring, to help with mixing and degassing. The sulfur precursor is prepared by mixing the sulfur powder and 7.5 mL OLA into a vial. During the mixing of the solution, a color change from yellow to clear orange indicates that reduction of S^0 into S^{2-} is taking place. This is the third role of OLA that also act as reducing agent through the doublet of the nitrogen. Meanwhile the atmosphere of the flask is changed to nitrogen, and the temperature tuned to 150°C. The sulfur precursor is quickly added to the 3-neck flask through a septum stopper using a syringe, to avoid the introduction of air in the system. The speed at which the sulfur precursor is added to the $PbCl_2$ in OLA mixture is critical, and should be as fast as possible to have a single nucleation step and obtain monodispersed CQDs.

The goal of the synthesis was obtaining nanocrystals with absorption edge at $\lambda = 1.7$ μm (or wavenumber at around 6000 cm^{-1}, hence the name "PbS 6k"), and for this purpose the growth step was carried out for 15 minutes at 150°C. The growth of NCs was quenched using a solution prepared with 9 mL hexane and 1 mL of oleic acid, which were added using a syringe, but at a slow rate to prevent hexane from boiling, which could lead to the deposition of nanocrystals on the glass column. The solution was washed twice adding ethanol, agitating the solution and then centrifuging. During centrifugation, the NCs precipitate forming a pellet at the bottom of the tube, leaving a supernatant which is discarded. After washing, the nanocrystals pellet is dissolved in toluene, giving a solution of dark brownish color. The solution is centrifuged one final time, and during this step the stable crystal of the appropriate size remained dispersed in toluene, while the ones that are too big precipitate, forming a pellet which is to be discarded. Cleaning is especially critical to later use nanocrystals in devices. We aim to keep just the right quantity of ligands to passivate the surface and preserve colloidal stability, but an excessive amount will be detrimental to transport. The synthesis is now complete, and the nanocrystal in colloidal solution can be transferred to a tight vial and stored in a freezer to maximize the shelf life.

The absorption spectrum of the CQDs (Figure 12) was measured using an attenuated total reflectance (ATR) detector installed in the FTIR spectrometer. The working principle of the ATR relies on a high refractive index crystal (diamond in this case) on which a drop of solution containing the nanocrystals is deposited. IR light is directed towards the crystal at an angle which ensures total internal reflection in the crystal. When this happens, an evanescent wave propagates for a few micrometers towards the sample, which in turn absorbs energy from the wave at specific wavelengths that allow for interband absorption inside of the material. When the reflected light is collected by the FTIR detector, the spectral information of the sample can be recovered.

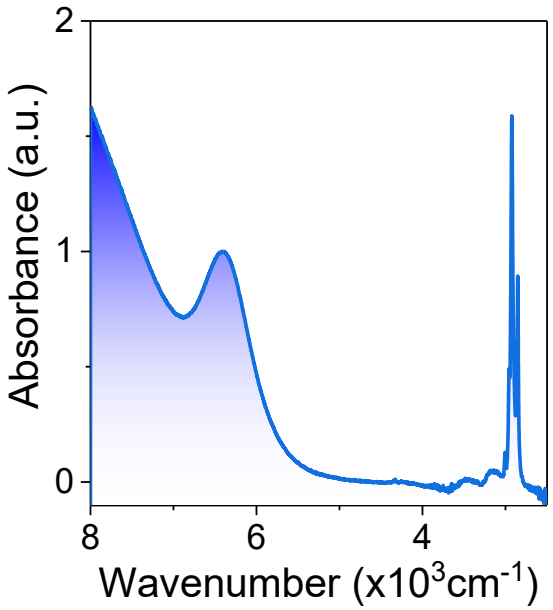

Figure 12: absorbance spectrum of the PbS CQDs. The peak at 3k is due to C-H bonds in the long ligands. The excitonic peak is localized at 6.4k, while the absorption edge is at 5.8k.

4.1.3 Preparation of a CQDs ink

In devices, nanocrystals are used under thin film form. A liquid phase ligand exchange is performed by combining the CQDs provided by our chemist engineer, an exchange solution, and DMF into a vial. The exchange solution contains 30 mg of $HgCl_2$, 18 mL of DMF, and 2 mL of mercaptoethanol (MPOH). After ligand exchange, the CQDs solution is washed twice with hexane to remove residue of long ligands and aggregated particles, and the NCs are finally precipitated adding toluene and centrifuging. After centrifugation a pellet is formed on the bottom of the vial, which has to be mechanically distributed along the walls of the tube for an easier evaporation of the leftover solvent. Finally, DMF is added to the dried QDs to redisperse them, forming an ink which can be spin coated.

CQD thin films are realized using spin coaters. A vacuum pump is connected to this instrument to create a tight seal between the sample and the chuck on which it is mounted. A small quantity of CQD ink is poured over the substrate using a pipet. Spin coating parameters such as spin time, velocity and acceleration can be tuned to obtain films of the desired thickness. In most of my devices, a film thickness of 300 nm allows for a good compromise between absorbed photons and transport properties.

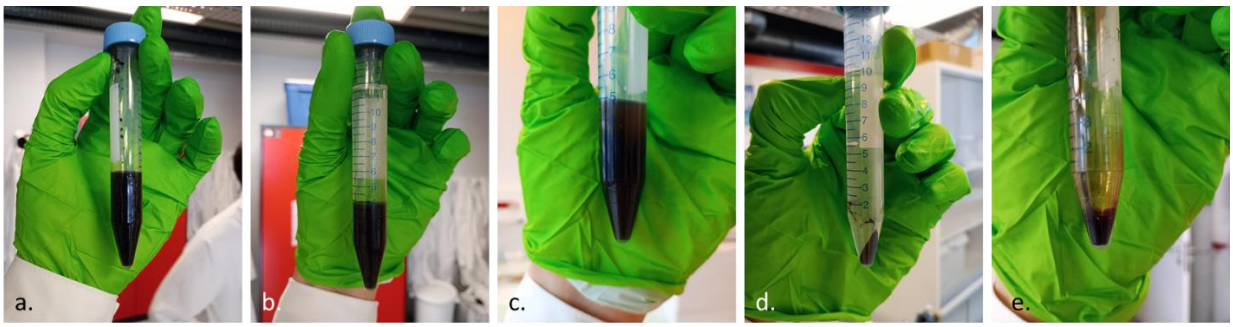

Figure 13: main steps in the preparation of a CQD ink. a. ligand exchange. b. hexane washing. c. precipitation with toluene. d. formation of the CQD pellet. e. redispersion in DMF.

The inks are stored inside of a freezer. Each time a new ink is prepared, the parameters for spin coating are adjusted, since variations in the concentration of the solution translate to different film thickness.

4.2 Sample characterization

In the following subsections the main figures of merit which can be calculated for a detector, along with the experimental setup to obtain them and the results of my work are described.

4.2.1 Dark current

An ideal photodetector is a good conductor when illuminated, and an insulator when kept in dark. In reality, a detector will exhibit a current even though there are no photogenerated carriers. This is known as *dark current*, and during the design of a device, one of the objectives is its minimization. A high dark current is detrimental for the sensitivity of a device, and it lowers the SNR. The primary sources of dark current are thermally activated carriers and impurity or defects inside of the bulk material.

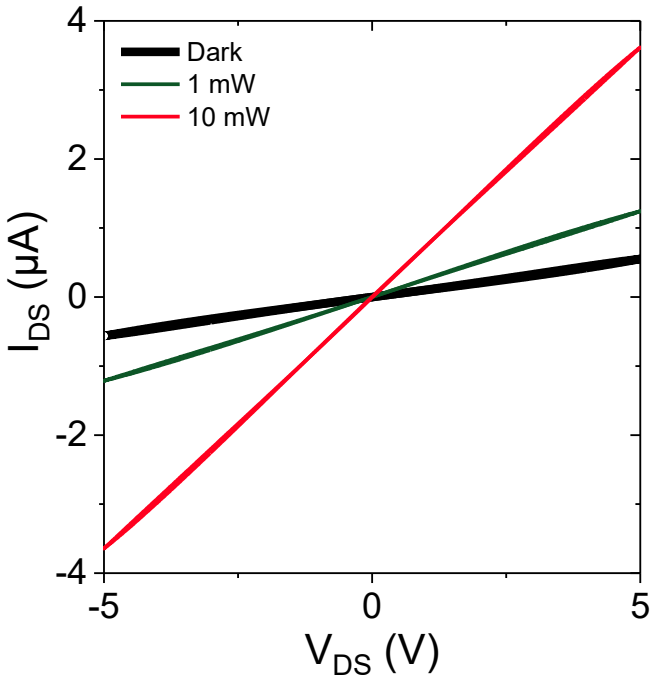

Figure 14: IV curves in dark and under illumination of a photoconductor based on a HgTe 6k film. For the curves under illumination, a 1.55 μm laser was used. The room temperature resistance goes from 9 MΩ for the detector kept in dark, to 1.4 MΩ when the power of the laser is set to 10 mW.

MWIR photoconductors need to be operated under a non-zero bias, so they present a large dark current, which causes the SNR to be intrinsically low and the photocurrent hard to detect. For this reason, for the characterization of the photoresponse of my devices I had to rely on complicated techniques and experimental setups. For the evaluation of the photocurrent a lock-in amplifier was used. This instrument is design for the detection of weak signals, and its working principle relies on a reference signal with the same frequency and waveform of the target signal. The latter is multiplied with the reference, to obtain an amplification of the components which are in phase. The signal is finally integrated over a number of periods, to average out the noise. For photocurrent measurements, the reference signal I used is the reference coming from the optical chopper controller, which will be treated later.

4.2.2 Noise

The dark current presents random temporal fluctuations, commonly referred to as *noise current*. Noise in a photodetector is caused by a number of factors:

- **Thermal noise:** is caused by random thermal fluctuations in the device, causing the activation of carriers.

- **Generation-recombination (GR) noise:** generated by the random fluctuation in the rates of generation and recombination. This noise is directly proportional to the dark current.
- **Flicker noise:** also called $1/f$ noise, is inversely proportional to the modulation frequency, and it's normally attributed to defects and impurities in the detector.

If the device is cooled to cryogenic temperatures, thermal generation will be strongly suppressed. This is also true for GR and flicker noise, since they both scale like the dark current, which is reduced at low temperature. As a consequence, the detector will be able to detect weaker signals. For this reason, many MWIR and LWIR detectors are cooled during operation.

Noise current can be evaluated using a frequency analyzer. The signal is first amplified using a low noise current amplifier. Using Fast Fourier Transform techniques, the noise is separated into its spectral components, allowing to discriminate the dominant noise source in the device.

The preparation of the setup for a noise measurement consisted in removing all the possible external sources of noise. Particular care has to be used when connecting all the different elements of the experimental setup, to ensure that a common electrical ground is well defined. Aluminum foil was used to create a Faraday cage around the elements of the circuit sensitive to external electromagnetic radiation, such as the I/V converter and amplifier. With all of these precautions, I was able to detect values of noise down to a few hundred $fA \cdot Hz^{-0.5}$. Lower values of noise ($\sim 10^{-14}$) can be reached with more resistive devices, indicating that the measurement is setup limited.

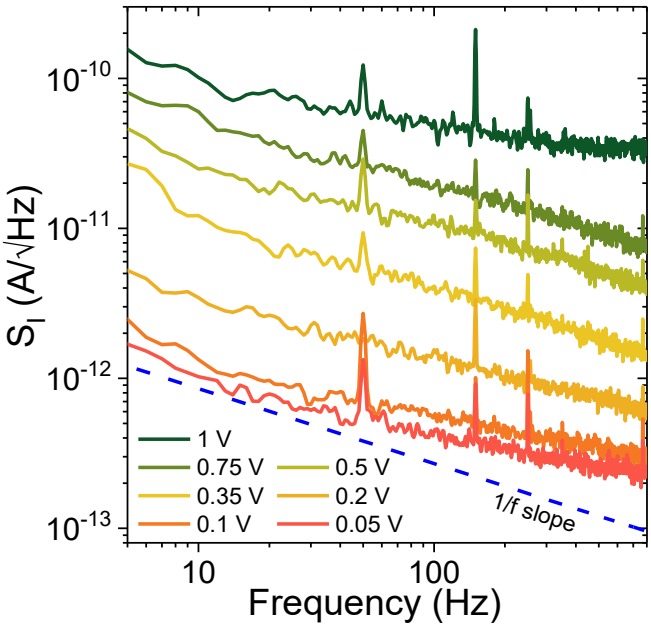

Figure 15: noise spectrum of a photoconductor based on a 150 nm thick film of HgTe/CdS core-shell CQDs. The value of the noise current increases linearly with the applied bias V_{DS}. Flicker noise is domninant in this device.

When evaluating the quality of a detector, responsivity gives a first general indication on the ability to transduce incoming photon into an electrical signal, but it does not consider the noise in the device. For this reason, the most relevant figure of merit for a sensor is the *detectivity* D^*, directly related to the signal to noise ratio, and expressed by

$$D^* = \frac{R\sqrt{A_d}}{S_I}$$

where S_I is the measured noise current density.

4.2.3 Activation energy

Most of the devices fabricated were characterized inside of a cryostat, because noise is reduced as low temperatures are reached. For this reason, experimental investigation usually began with mounting the device to be studied inside of a cryostat connected to a liquid helium compressor, and cooling it down to 80 K. During this procedure, the sample is connected to a Keithley 2634B. During cooling, a constant bias is applied between drain and source contacts of the device, drawing a current between the two electrodes. This current can be measured and plotted as a function of the temperature of the sample, which is monitored by a temperature controller.

Experimental results (Figure 16) show how the I vs T curve for detectors based on HgTe nanocrystals exhibits an exponential decay behavior between 295 K and 200 K. This temperature interval is the one over which nearest-neighbor hopping transport dominates, while at lower temperatures variable range hopping (VRH) takes place due to the fact that k_bT becomes smaller that the characteristic disorder energy. VRH happens when carriers prefer to hop to final states with energy closer to the one of the initial states, even though these may be localized in QDs which are further away with respect to those of neighboring NCs. The x axis shows 1000/T to scale the x axis for a more convenient visualization.

The exponential portion of the I(T) plot can be fitted with an Arrhenius curve in order to obtain the activation energy E_a, which represents the energy barrier that carriers have to overcome to hop from one site to another. This is done by fitting the dark current data for temperatures in the 295 K – 200 K range with an Arrhenius-like model, represented by

$$y = Ae^{-\frac{E_a}{RT}} = Ae^{-\frac{x}{t}}$$

Through the fitting parameter t, the activation energy E_a is immediately obtained.

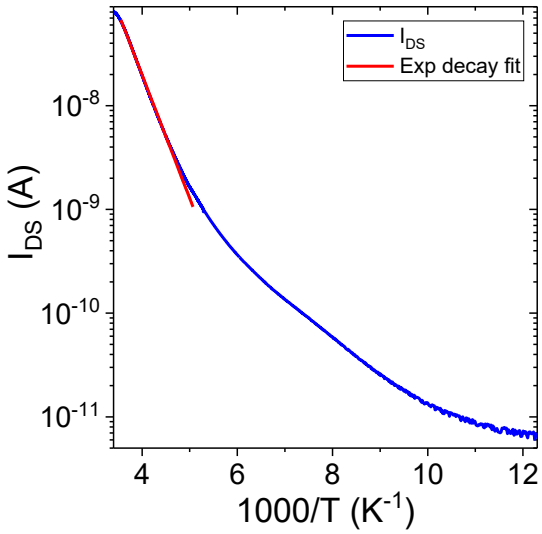

Figure 16: I(T) curve of a 300 nm thick HgTe 6k film in blue. In red, exponential decay fitting of the first part of the curve.

Concerning the sample Figure 16, the extrapolated activation energy is 336 meV. The higher the activation energy, the stronger the reduction of dark current when the device is cooled. Thus, having a device with a high activation energy is desirable for a fast reduction of the dark current, without impacting the electron mobility. The value of the activation energy is expected to be around half of the bandgap for an ideal intrinsic semiconductor. In real semiconductors, the presence of deep trap states,

located close to the middle of the energy gap, causes the values of the activation energy to be lower than $E^*/2$. This is confirmed from the values for E_a extracted from Figure 16, where $E_a < E^*/2$ (= 371 meV).

4.2.4 Responsivity

Responsivity is a critical parameter which measures the effectiveness of photodetectors in converting light into an electrical signal. It is defined as the electrical output per optical input, and its unit of measurement is A/W, thus we can simply express it as $R(\lambda) = I_{ph}/P_{in}$. This quantity may depend on the incident photon flux. In general, the higher the flux, the weaker the response of the sensor. Blackboy radiation sources are commonly used to evaluate R, since they are a good representation of typical scenes in IR imaging (i.e., broadband emission). The power emitted by a blackbody can be evaluated using:

$$P_{in}^{BB} = A_d \cos(\theta) \sin^2(\varphi) \int_{\lambda_{min}}^{\lambda_{max}} \frac{2hc^2}{\lambda^5} \frac{1}{e^{hc/\lambda k_b T}} \, \mathrm{d}\lambda$$

where A_d is the photoactive area of the device, θ is the angle between the source and the detector, φ is the half angle of view under which the blackbody illuminates the detector, λ_{min} and λ_{max} are the border wavelengths for integration (usually corresponding to the cutoff wavelengths of the filter (see Figure 17) and device, respectively), h is Plank's constant, c the speed of light, k_b is Boltzmann's constant, and T is the temperature of the blackbody. The photocurrent can be easily measured by chopping the signal with a square wave and connecting the output of the detector to a lock-in amplifier.

The detectors were always mounted inside of a cryostat chamber, to study the behavior of the parameters versus temperature. The cryostat at INSP is equipped with two zinc selenide (ZnSe) windows. ZnSe is a wide bandgap semiconductor with a transmission range (0.6 μm to 16 μm) which allows for the attenuation of the high energy part of the visible spectrum, while leaving IR radiation relatively undisturbed. The attenuation of the signal that travels through these windows have to be taken into account when calculating P_{in}^{BB}, by introducing an attenuation factor. The radiation source can vary between a laser or a blackbody, but for the reason mentioned above, blackbody radiation was often preferred.

IR detectors are often subject to luminous signals which vary in time, for this reason a modulation of light coming from the IR source was induced either electronically (using a pulsed laser) or mechanically (by means of an optical chopper). In most of my measurements, the frequency was set to 100 Hz using an optical chopper, which consists of a metallic punctured blade placed between the IR source and the detector. A 1.9 μm germanium (Ge) filter was placed in front of the cryostat window to set a precise cutoff wavelength for the calculation of the optical power impinging on the sample. The detector is placed inside of the cryostat and silver paste is used to have a good contact between the copper tips on the sample holder and the electrodes on the sample, making sure that the contacts hold when vacuum is generated inside of the chamber. The signal emitted by the sample is brought to lock-in amplifier through shielded BNC cables. The lock in amplifier can be used to apply a V_{DS}, as well as for an easy evaluation of both dark current and photocurrent flowing in the detector.

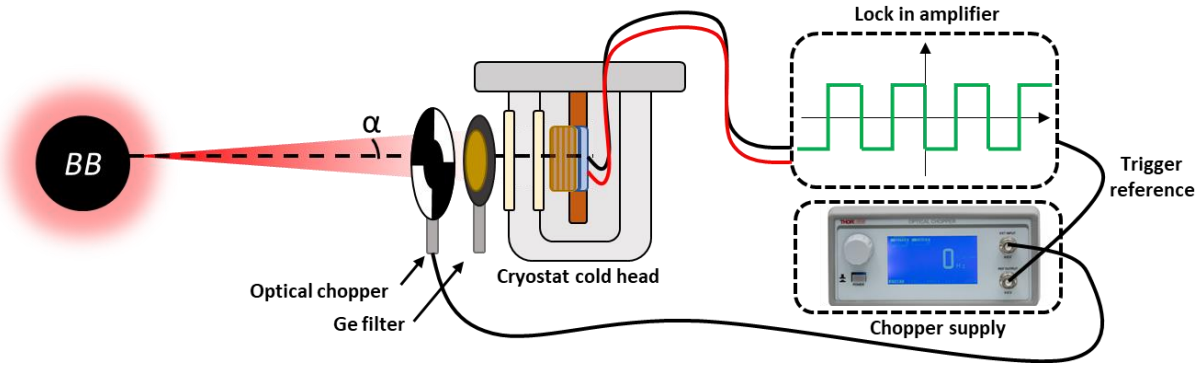

Figure 17: illustration of the setup for a photocurrent measurement. The incidence angle θ in this representation is null, as the setup is realized to obtain normal incidence. The chopper supply reference is fed to the lock-in amplifier to multiply the signal form the detector placed inside of the cryostat.

I explored the behavior of the responsivity versus temperature, to gain information on the temperature at which the performance of HgTe CQD based detectors is best. The measurements were conducted under illumination from a blackbody source at 980 °C, and for different values of V_{DS}. The best operating temperature was found to be in the 100-150 K temperature range, regardless of the bias. The reason for the presence of a maximum is due to the interplay between charge carrier mobility and population of trap states inside of the bandgap. Electron mobility is thermally activated inside of a nanocrystal film, thus a temperature which is too low will cause a drop in photocurrent. On the other hand, as the temperature is raised above 150 K, the capture rate of trap states in the bandgap increases, causing a drop in the number of photogenerated carriers collected at the electrodes. A linear behavior of the responsivity vs. bias can be noticed when looking at Figure 18 b. This is due to the higher number of photogenerated carriers collected at the electrodes under a stronger electric field.

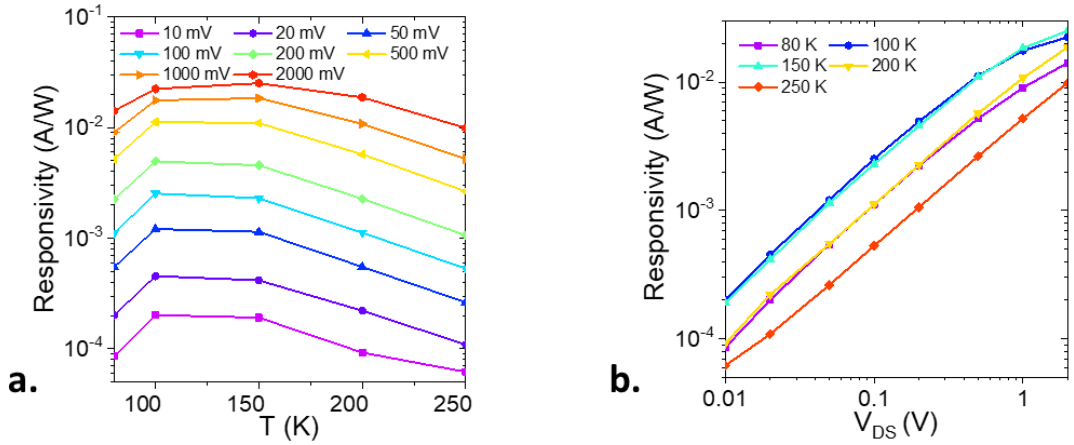

Figure 18: a. responsivity vs temperature for different values of V_{DS}. b. responsivity vs bias at different temperatures.

4.2.5 Spectral characterization

The size of the nanocrystals has a direct influence on the optoelectronic properties of the final device. In order to make sure that the fabricated detectors are sensitive to radiation of a specific wavelength, absorption experiments can be performed, using a FTIR spectrometer. This machine allows to perform absorption and transmission experiments using infrared light, but it can be used to gain information on the spectral response of a device. A scheme of the experimental setup for the spectral characterization is shown in Figure 19. The detector is biased by a transimpedance amplifier, which is also used to convert the current signal into a voltage, which can be used by the FTIR. The latter uses a Michelson interferometer and a movable mirror to produce modulated infrared light, which will reach the detector,

generating a photocurrent. This current is fed back to the FTIR, which synchronizes the device response and the mirror, ultimately calculating the Fourier transform. Finally, the photocurrent spectrum as a function of the wavenumber is displayed.

The spectral response allows to determine the value of the absorption edge of the active material, which delimits the transition between transparency to significant absorption of light from the sensor. The absorption edge of an infrared detector is defined as the energy (or wavelength) at which the absorption coefficient of the active material shows a sharp increase. For a semiconductor device, this energy corresponds to the bandgap of the material.

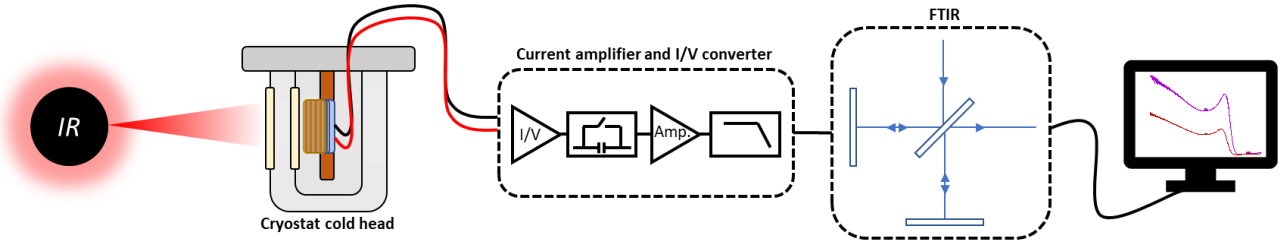

Figure 19: illustration of the setup for a photocurrent spectrum measurement using a FTIR spectrometer.

Since most sensors are operated at cryogenic temperatures, it is relevant to track the shift of the band edge with temperature. The experimental results are in accordance with ref. [21], and show a temperature dependance of the spectral response which is inverted with respect to standard semiconductors. The band edge red-shifts as the temperature is decreased, meaning that the optical bandgap is decreased at low temperatures.

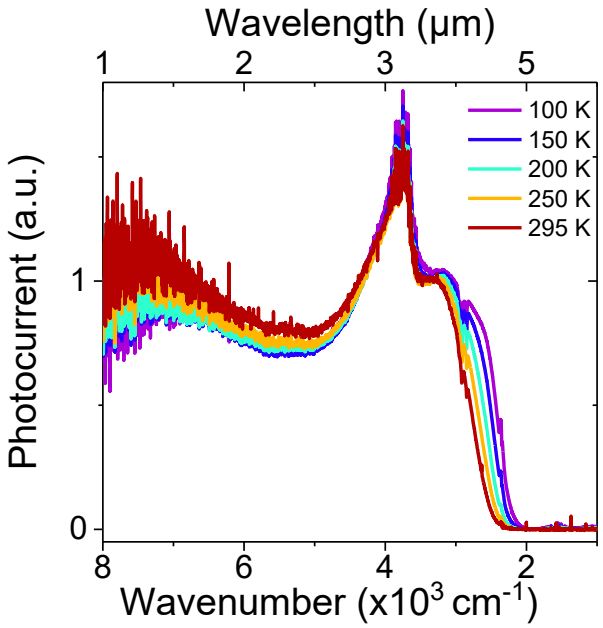

Figure 20: normalized photocurrent spectrum of a 100 nm thick film of HgTe 3k under IR light illumination. This film was used as the active layer of a photoconductor on a glass substrate. The absorption edge is red shifted as the temperature is lowered. The absorption peak at 4k is a feature due to the background which was poorly collected.

Further measurements to evaluate the dependence of the drain-source bias on the position of the absorption edge showed no dependence at all.

5 Conclusions and perspectives

This report is devoted to the presentation of the techniques for the fabrication and characterization of mid-wave infrared photodetectors. This experience allowed me to dive deeply in the world of experimental physics, and to discover the field of infrared sensing. I gained experience with the instrumentation of an optoelectronics laboratory, where I was able to operate a cryostat to conduct temperature, gate bias, and frequency resolved measurements. I also acquired confidence in working inside of a cleanroom environment, where I became familiar with photolithographic and deposition processes, for the fabrication of detectors starting from the bare substrate. I was able to become confident in working inside of a glovebox, which I used for all the fabrication that required an oxygen free environment. Lastly, during my internship I learned how to work inside of a chemistry laboratory, to handle chemicals for the preparation of CQD inks, to be deposited for the formation of photoconductive thin films, on which all of my devices were based.

I was able to determine the absorption spectrum of the as-synthetized CQD solutions, and concerning the devices I fabricated, I was able to measure the most significant figures of merit, such as noise current density, photocurrent spectrum, responsivity and activation energy.

The main ambition of this work is the fabrication of low-cost infrared detectors based on HgTe nanocrystals. This technology is still at an early stage, and more progress is to be done to reach the maturity for integration in cameras. Further research can give more insight on the electronic structure of the active material and on the transport mechanisms inside of it. Different device geometries can be explored to address the limitations that affect modern detectors.

References

(1) Murray, C. B.; Norris, D. J.; Bawendi, M. G. Synthesis and Characterization of Nearly Monodisperse CdE (E = Sulfur, Selenium, Tellurium) Semiconductor Nanocrystallites. *J. Am. Chem. Soc.* **1993**, *115* (19), 8706–8715. https://doi.org/10.1021/ja00072a025.

(2) Klipstein, P. C. XBn and XBp Infrared Detectors.

(3) Rossetti, R.; Nakahara, S.; Brus, L. E. Quantum Size Effects in the Redox Potentials, Resonance Raman Spectra, and Electronic Spectra of CdS Crystallites in Aqueous Solution. *J. Chem. Phys.* **1983**, *79* (2), 1086–1088. https://doi.org/10.1063/1.445834.

(4) Ekimov, A. I.; Onushchenko, A. A. Quantum Size Effect in Three-Dimensional Microscopic Semiconductor Crystals. *Sov. J. Exp. Theor. Phys. Lett.* **1981**, *34*, 345.

(5) Rinnerbauer, V.; Hingerl, K.; Kovalenko, M.; Heiss, W. Effect of Quantum Confinement on Higher Transitions in HgTe Nanocrystals. *Appl. Phys. Lett.* **2006**, *89* (19), 193114. https://doi.org/10.1063/1.2387110.

(6) Gréboval, C.; Darson, D.; Parahyba, V.; Alchaar, R.; Abadie, C.; Noguier, V.; Ferré, S.; Izquierdo, E.; Khalili, A.; Prado, Y.; Potet, P.; Lhuillier, E. Photoconductive Focal Plane Array Based on HgTe Quantum Dots for Fast and Cost-Effective Short-Wave Infrared Imaging. *Nanoscale* **2022**, *14* (26), 9359–9368. https://doi.org/10.1039/D2NR01313D.

(7) Gréboval, C.; Chu, A.; Goubet, N.; Livache, C.; Ithurria, S.; Lhuillier, E. Mercury Chalcogenide Quantum Dots: Material Perspective for Device Integration. *Chem. Rev.* **2021**, *121* (7), 3627–3700. https://doi.org/10.1021/acs.chemrev.0c01120.

(8) Nag, A.; Kovalenko, M. V.; Lee, J.-S.; Liu, W.; Spokoyny, B.; Talapin, D. V. Metal-Free Inorganic Ligands for Colloidal Nanocrystals: S^{2-}, HS^{-}, Se^{2-}, HSe^{-}, Te^{2-}, HTe^{-}, TeS_3^{2-}, OH^{-}, and NH_2^{-} as Surface Ligands. *J. Am. Chem. Soc.* **2011**, *133* (27), 10612–10620. https://doi.org/10.1021/ja2029415.

(9) Dolzhnikov, D. S.; Zhang, H.; Jang, J.; Son, J. S.; Panthani, M. G.; Shibata, T.; Chattopadhyay, S.; Talapin, D. V. Composition-Matched Molecular "Solders" for Semiconductors. *Science* **2015**, *347* (6220), 425–428. https://doi.org/10.1126/science.1260501.

(10) Guyot-Sionnest, P. Electrical Transport in Colloidal Quantum Dot Films. *J. Phys. Chem. Lett.* **2012**, *3* (9), 1169–1175. https://doi.org/10.1021/jz300048y.

(11) Dang, T. H.; Cavallo, M.; Khalili, A.; Dabard, C.; Bossavit, E.; Zhang, H.; Ledos, N.; Prado, Y.; Lafosse, X.; Abadie, C.; Gacemi, D.; Ithurria, S.; Vincent, G.; Todorov, Y.; Sirtori, C.; Vasanelli, A.; Lhuillier, E. Multiresonant Grating to Replace Transparent Conductive Oxide Electrode for Bias Selected Filtering of Infrared Photoresponse. *Nano Lett.* **2023**, *23* (18), 8539–8546. https://doi.org/10.1021/acs.nanolett.3c02306.

(12) Lhuillier, E.; Keuleyan, S.; Zolotavin, P.; Guyot-Sionnest, P. Mid-Infrared HgTe/As2S3 Field Effect Transistors and Photodetectors. *Adv. Mater.* **2013**, *25* (1), 137–141. https://doi.org/10.1002/adma.201203012.

(13) Gréboval, C.; Noumbe, U.; Goubet, N.; Livache, C.; Ramade, J.; Qu, J.; Chu, A.; Martinez, B.; Prado, Y.; Ithurria, S.; Ouerghi, A.; Aubin, H.; Dayen, J.-F.; Lhuillier, E. Field-Effect Transistor and Photo-Transistor of Narrow-Band-Gap Nanocrystal Arrays Using Ionic Glasses. *Nano Lett.* **2019**, *19* (6), 3981–3986. https://doi.org/10.1021/acs.nanolett.9b01305.

(14) Chen, M.; Xue, X.; Qin, T.; Wen, C.; Hao, Q.; Tang, X. Universal Homojunction Design for Colloidal Quantum Dot Infrared Photodetectors. *Adv. Mater. Technol.* **2023**, *8* (16), 2300315. https://doi.org/10.1002/admt.202300315.

(15) Qin, T.; Mu, G.; Zhao, P.; Tan, Y.; Liu, Y.; Zhang, S.; Luo, Y.; Hao, Q.; Chen, M.; Tang, X. Mercury Telluride Colloidal Quantum-Dot Focal Plane Array with Planar p-n Junctions Enabled by in Situ Electric Field–Activated Doping. *Sci. Adv.* **2023**, *9* (28), eadg7827. https://doi.org/10.1126/sciadv.adg7827.

(16) Rastogi, P.; Izquierdo, E.; Gréboval, C.; Cavallo, M.; Chu, A.; Dang, T. H.; Khalili, A.; Abadie, C.; Alchaar, R.; Pierini, S.; Cruguel, H.; Witkowski, N.; Utterback, J. K.; Brule, T.; Xu, X. Z.; Hollander, P.; Ouerghi, A.; Gallas, B.; Silly, M. G.; Lhuillier, E. Extended Short-Wave Photodiode Based on CdSe/HgTe/Ag2Te Stack with High Internal Efficiency. *J. Phys. Chem. C* **2022**, *126* (32), 13720–13728. https://doi.org/10.1021/acs.jpcc.2c02044.

(17) Luo, Y.; Tan, Y.; Bi, C.; Zhang, S.; Xue, X.; Chen, M.; Hao, Q.; Liu, Y.; Tang, X. Megapixel Large-Format Colloidal Quantum-Dot Infrared Imagers with Resonant-Cavity Enhanced Photoresponse. *APL Photonics* **2023**, *8* (5), 056109. https://doi.org/10.1063/5.0145374.

(18) Keuleyan, S.; Lhuillier, E.; Guyot-Sionnest, P. Synthesis of Colloidal HgTe Quantum Dots for Narrow Mid-IR Emission and Detection. *J. Am. Chem. Soc.* **2011**, *133* (41), 16422–16424. https://doi.org/10.1021/ja2079509.

(19) Hines, M. A.; Scholes, G. D. Colloidal PbS Nanocrystals with Size-Tunable Near-Infrared Emission: Observation of Post-Synthesis Self-Narrowing of the Particle Size Distribution. *Adv. Mater.* **2003**, *15* (21), 1844–1849. https://doi.org/10.1002/adma.200305395.

(20) Moreels, I.; Lambert, K.; Smeets, D.; De Muynck, D.; Nollet, T.; Martins, J. C.; Vanhaecke, F.; Vantomme, A.; Delerue, C.; Allan, G.; Hens, Z. Size-Dependent Optical Properties of Colloidal PbS Quantum Dots. *ACS Nano* **2009**, *3* (10), 3023–3030. https://doi.org/10.1021/nn900863a.

(21) Lhuillier, E.; Keuleyan, S.; Guyot-Sionnest, P. Optical Properties of HgTe Colloidal Quantum Dots. *Nanotechnology* **2012**, *23* (17), 175705. https://doi.org/10.1088/0957-4484/23/17/175705.